Contents lists available at ScienceDirect

Journal of Trace Elements in Medicine and Biology

journal homepage: www.elsevier.com

Toxicology

New insights into the metal partitioning in different microphases of human gallstones

Annika Parviainen[a, *], Manuel Jesús Roman Alpiste[a], Claudio Marchesi[a, b], Juan Manuel Suárez-Grau[c], Rafael Pérez-López[d]

[a] Instituto Andaluz de Ciencias de la Tierra (IACT), CSIC-UGR, Avda. de las Palmeras 4, E-18100, Armilla, Granada, Spain
[b] Departamento de Mineralogía y Petrología, UGR, Avda. Fuentenueva s/n, E-18002 Granada, Spain
[c] Riotinto Hospital, Avda. La Esquila 5, E-21660, Minas de Riotinto, Huelva, Spain
[d] Department of Earth Sciences & Research Center on Natural Resources, Health and the Environment, University of Huelva, Campus 'El Carmen', E-21071 Huelva, Spain

ARTICLE INFO

Keywords:
Biomineralization
Cholesterol
Bilirubinate
Ca carbonate
Ca phosphate
Pigment stone

ABSTRACT

Chronic metal exposure, e.g. from metal mining, may cause accumulation of metals in soft and hard tissues, and in developing biomineralizations in the human body. Gallstones are biomineralizations formed in the gallbladder which are able to trap trace elements from the bile. Laser Ablation-Inductively Coupled Plasma-Mass Spectrometry (LA-ICP-MS) was used to analyze gallstone cross-sections to trace the elemental abundances and correlate them with the principal phases constituting gallstones, namely cholesterol, Ca bilirubinate salts, Ca carbonate, and Ca phosphate. Five different types of gallstones (pure, mixed, and composite cholesterol stones, pigment stone, and carbonate stone) were chosen according to a previous classification based on phase characterization by different spectroscopic and microscopic techniques. These data were combined with bulk solution ICP-MS/OES analyses for total elemental concentrations. The results indicated that cholesterol has a zero capacity to retain elements except for Ca. Hence, pure cholesterol stones contained the lowest bulk metal concentrations, and the metals were found in the scarce carbonate and phosphate phases in these calculi. Calcium and trace element concentrations increased in other types of gallstones along with increasing amount of bilirubinate, carbonates and phosphates; pigment stones being the most enriched in metals. Phosphates were the principal carriers of Ca, P, Na, Mg, Mn, Fe, Pb, and Cd, whereas carbonate phases were enriched in Ca, Mg, Na, and Mn in order of decreasing abundance. Bilirubinate on the other hand was enriched in Ca, Cu, Ag, and Ni. The higher trace metal affinities of bilirubinate and phosphate explain the elevated metal concentrations observed in the pigment stones. These results give new insight to the trace metal behavior in the gallstone formation and the metal accumulation in the human body, validating the possible use of these biomineralizations as a proxy for exposure to metal pollution.

1. Introduction

Gallstone formation (cholelithiasis) is a common disease in which biomineralizations, mainly composed of cholesterol, Ca bilirubinate, Ca carbonate, and Ca phosphate, and some other minor phases, develop in the gallbladder. The bile fluids of the gallbladder naturally contain trace elements such as, Al, Ca, Cr, Cu, Fe, Mn etc., and they are eliminated from human body through bile discharge [1,2]. There are indications that metals can play a role in the gallstone formation and elevated concentrations of Cu, Cd, Ni, Cr, and Pb in serum, bile, and gallbladder tissue have been shown to have a strong relation with gallbladder cancer [3,4]. Additionally, consumption of drinking water contaminated by metals is possibly linked to gallbladder diseases [5]. However, more evidence is needed on how chronic metal exposure may influence on the gallstone formation, metal accumulation in them, and on the related gallbladder diseases. Previous studies have indicated that different types of gallstones may contain varying concentrations of metals and that especially pigment stones exhibit high amounts of metals [6–14]. Hence, these biomineralizations can be considered as long-term traps for metals, yet it remains unclear in which phases and in what form the metals appear.

* Corresponding author.
Email addresses: aparviainen@iact.ugr-csic.es (A. Parviainen); mj.roman@csic.es (M.J.R. Alpiste); claudio@ugr.es (C. Marchesi); graugrau@gmail.com (J.M. Suárez-Grau); rafael.perez@dgeo.uhu.es (R. Pérez-López)

https://doi.org/10.1016/j.jtemb.2017.09.013
Received 18 July 2017; Received in revised form 15 September 2017; Accepted 15 September 2017
Available online xxx
0946-672/

Up to day, the lack of high precision techniques has prevented the detailed study of metal partitioning in biological samples, but Laser Ablation-Inductively Coupled Plasma-Mass Spectrometry (LA-ICP-MS) offers a powerful technique for the microanalysis of trace elements in a great variety of organic and inorganic materials. For instance, this technique has been used in the study of kidney stones [15–17]. Semi-quantitative elemental distribution by LA-ICP-MS in combination with bulk elemental analysis by solution ICP-MS can be used to evaluate the relative elemental abundances of metals and their distribution among different phases.

The aim of this study was to investigate the trace element affinities of different types of gallstones and unveil the main host phases of the metal(loid)s. The cross-sections of five different types of gallstones were analyzed by LA-ICP-MS to identify the main carriers of metal(loid)s, and their respective bulk sample concentrations were analyzed by solution ICP-MS and ICP-OES (Optical Emission Spectrometry). The final purpose of this study, which is part of a larger research project investigating the impact of metal mining on humans in the Huelva region in SW Spain, is to validate the use of these biomineralizations to assess the impact of chronic exposure to metal pollution on humans.

2. Materials and methods

Five representative gallstone samples of different types of calculi based on previous classification [18] were selected, i.e. pure, mixed and composite cholesterol stones, a pigment stone, and a carbonate stone. The gallstone samples were supplied by the General Hospital of Riotinto in Huelva Province, SW Spain, under informed consent of the patients, and under approval of the Regional Ethical Committee of Huelva and of the Ethical Committee of the Spanish National Research Council (CSIC). The selected samples were previously photographed by optical microscope and characterized for mineralogical phase composition by bulk powder X-Ray Diffraction (XRD), Fourier Transformed Infra-Red Spectroscopy (FTIR), Micro-Attenuated Total Reflection FTIR (μ-ATR-FTIR), and Environmental Scanning Electron Microscopy with Energy Dispersive X-ray Spectroscopy (ESEM-EDS). Full description of the previous characterization can be found elsewhere [18].

The gallstone samples were first embedded in resin (Epofix) and cut in half using a slow-speed diamond saw exposing the central cross-section. The LA-ICP-MS analyses were performed on the specimen at the IACT (CSIC-UGR, Granada, Spain) using a Photon Machine excimer 193 nm laser coupled to an Agilent 8800 ICP-MS/MS. The analyzed elements include major elements and potentially toxic elements considered as contaminants derived from metal mining: Ag, As, Ca, Cd, Co, Cu, Fe, Mg, Mn, Na, Ni, P, Pb, and S. The ICP-MS/MS system offers the possibility to use a quadrupole filter before the reaction cell to remove potential isobaric interferences on some of the elements of interest, particularly the mono-isotope As. Preliminary experiments conducted provided satisfactory results in the Single Quad/No gas mode. Hence, mass shift and reaction gases were not necessary in LA-ICP-MS in this study. The optimized operating conditions of LA-ICP-MS are summarized in Table 1.

Internal standardization for the quantitative calculation of elemental concentrations was not feasible for these samples. We opted not to use an internal standard element (for instance Ca which is the most abundant element in gallstones) measured with another technique, e.g. electron micro-probe analysis, because the variation of Ca concentrations even within one microphase is considerable which could lead to significant errors in the result interpretation. Hence, the results of the LA-ICP-MS are presented as semi-quantitative, and merely approximated elemental abundances are discussed which is suitable to fulfill the objectives of this work. The NIST612 synthetic glass was used as external standard for the system set up, lenses tuning, and for drift correction. The measurements for NIST612 were performed under same conditions as for the samples. Blanks were measured for 40 s.

Table 1
Summary table of LA-ICP-MS equipment and optimized conditions of analysis.

Laser Ablation System		ICP-MS	
Model	PhotonMachines Analyte Excite 193	Model	Agilent 8800 QQQ
Type	Excimer	Type	Single Collector
Wavelength	193 nm	Forward Power	1550 W
Mode/Spot size	Raster/40 μm	Scanned Masses	Na^{23}, Mg^{24}, P^{31}, S^{32}, S^{34}, Ca^{43}, Ca^{44}, Mn^{55}, Fe^{56}, Co^{59}, Ni^{60}, Cu^{63}, Cu^{65}, As^{75}, Ag^{107}, Cd^{111}, Pb^{208}
Ablation Speed	5 μm/s	Integration Time	0.1 s each element
Fluence	10.5 mJ/cm^2	Sample Depth	4 mm
Raster Length	1 mm/segment	Ar Carrier Gas Flow	0.8 l/min
Washout Time	40 s	Analysis Mode	Time resolved Analysis
He Carrier Flow	0.8 l/min primary 0.2 l/min secondary		

A cross-section of each sample was studied under LA. Each cross-section consisted of a sequence of segments of approximately 1 mm in length covering the whole sample section. Hence, 2–11 segments were analyzed on each sample depending on the length of the sample cross-section. The external standard was run before and after every sample with the exception of larger samples with more than six segments in which case the external standard was also measured in the middle of the sample. Blanks were measured before and after every integration of external standard and sample segment.

Processing of the final data was performed using Iolite 2.5 software [19,20]. For the semi-quantitative calculation, NIST612, which contains multi-elements, was used for calculating the concentration conversion coefficient (K) separately for each element measured. This K-value was calculated by comparison of the sensibility ratios between sample and standard taking into consideration the instrumental drift. Due to the different matrix of the NIST glass in comparison to the measured material, the error in semi-quantitative values may increase. Using the standard concentration values, and using the same analysis conditions we assume that the volume of ablated material for both NIST and the unknown sample is similar and the ablation behavior is also the same. The limits of detection (LOD) were calculated for each element using the Iolite software (Table 2). The semi-quantitative LODs use the semi-quantitative sensitivity in absence of the internal standard. Hence, sensitivity is calculated using the simplified Longerich et al. [21] equation:

$$S = R_{ancal}/C_{ancal}$$

here R_{ancal} is the Count rate produced by X analyte in the reference material, C_{ancal} is the Concentration of X analyte in the reference material. Variables concerning to IS values are ignored on this method. Subsequently, the LOD is calculated using the Howell et al. [22] equation:

Table 2
Limits of detection for LA-ICP-MS (ppm).

	Ca	Mg	Na	P	S	Ag	As	Cd	Co	Cu	Fe	Mn	Ni	Pb
Limit of detection	1400	5.1	62	50	300	0.16	4.6	0.73	0.33	2.8	5.6	1.1	4.3	0.21

$$LOD = \frac{1}{S}\left[3 * 1\sigma_b * \sqrt{\left(\frac{1}{n_b} + \frac{1}{n_a}\right)}\right]$$

here S is the Sensitivity, σ_b is Standard deviation of the background, n_b is number of points in the background, n_a is number of measurements in the sample. The Howell method of calculation is used to avoid negative or infinite LODs when background yields zero value.

The elemental abundances in varying phases were estimated based on the identified phase distribution on the ablated lines. Special attention is paid on the discussion of As, Ag, Co, Cd, Cu, Fe, Ni, and Pb, which are considered as possible environmental contaminants derived from sulfide mining. Correlations of the elements were evaluated calculating Pearson correlation using IBM SPSS statistics 23 software.

Bulk element concentrations were determined using solution ICP-MS and ICP-OES techniques to evaluate the LA results and the element abundances. The elements analyzed were the same for solution technique as for LA: Ag, As, Cd, Co, Cu, Fe, Mn, Ni, and Pb were analyzed by ICP-MS, and Ca, Mg, Na, P, and S by ICP-OES. For this end, the respective sample halves were ground in an agate pestle mortar and 20 mg were digested in closed Savillex© in two cycles. First, 1 ml of purified HNO_3 (65%) and 0.1 ml of H_2O_2 (30%) were added and the vials were placed on a hotplate at 100 °C for 24 h. Subsequently, same amount of reagents were added and the vials were again placed on the hotplate for another 24 h in order to assure the total digestion of the samples. The ICP-MS analyses were carried out by an Agilent 8800 ICP-MS/MS at IACT, whereas ICP-OES analyses were performed using Varian 720-ES equipment at the Instrumental Technical Services of the Estación Experimental del Zaidín (CSIC, Granada, Spain). For the analyses by ICP-MS, Ag^{107}, Cu^{63}, Co^{59}, Fe^{56}, Mn^{55}, Ni^{60} were analyzed in He mode, whereas Cd^{111} and Pb^{208} were analyzed in No gas mode. For As^{75} reaction with O_2 was used to shift the mass to 91 in order to eliminate interference mainly by $ArCl^+$ which overlaps with mass 75. Compositions were corrected for contributions from procedural blanks and standards were run to control the quality of the solution analysis. The available standards that best represent gallstone samples are very limited and attention was paid in the selection of these materials. Bone meal (NIST1468 provided by the National Institute of Standards & Technology) and limestone (JLs-1 provided by the Geological Survey of Japan) were chosen as standards and show compositions similar to certified values (Table 3; exception of Na in JLs-1 for very low concentration). The bone meal represents the organic sample matrix with phosphates, whereas limestone represents the carbonate phases.

3. Results

3.1. Pure cholesterol stone

The pure cholesterol stone sample was composed of cholesterol and of merely traces of Ca bilirubinate, Ca carbonate and Ca phosphate (Fig. 1; [18]). The elemental determination by LA-ICP-MS was performed over cross-sections of two cholesterol grains in the same calculus and the respective elemental profiles are plotted in Fig. 1. Generally speaking, the pure cholesterol stone was poor in trace elements (Table 3). Calcium was the only element detected over the entire lines analyzed, while the other elements were merely observed in association with carbonates and phosphates. The Ca peaks together with the highest P peaks (up to 13 wt.%) were interpreted as phosphate grains while Ca peaks with lower P concentrations (average 1 wt.%) were associated to carbonate (Fig. 1B). The ESEM-EDS analysis revealed that carbonate phases may contain traces of P. Thus, these lines were principally composed of cholesterol (89%), whereas carbonate and phosphate phases together accounted for approx. 11% of the analyzed profile (Fig. 2A). Calcium was positively correlated with P (r = 0.583), Mg (r = 0.634), Mn (r = 0.535), and Na (r = 0.533). Among trace elements, Cu was the most abundant (average 1440 and 2070 ppm in carbonate and phosphate, respectively) and correlated with Na (r = 0.757) and other minor elements such as Fe (r = 0.656; 49.1 and 73.6 ppm, respectively) and Ni (r = 0.666; 21.8 and 39.9 ppm, respectively). The carbonate and phosphate phases contained low concentrations of Pb (1.89 and 5.02 ppm, respectively) and Ag (2.24 and 2.19 ppm, respectively), while As, Cd, Co, and S were not detected. These results are in accordance with the bulk metal concentrations which exhibited Ag, As, Co, Cd, and Ni below detection limit (BDL) and very low concentrations for Fe and Pb (Table 3).

3.2. Mixed cholesterol stone

The mixed cholesterol stone presented a composition very similar to the pure cholesterol stone with cholesterol as the main phase, though Ca carbonate and phosphate were slightly more abundant in comparison to the pure cholesterol stone (Fig. 3; [18]). This is also visible in the elemental profiles presented in Fig. 3 representing the corresponding LA raster line. Cholesterol as the major phase covered 86% of the ablated line, whereas carbonates and phosphates comprised 14% of the profile (up to 40 wt.% Ca and 2 wt.% P). Here the highest Ca and P peaks were associated to phosphates (corresponding to 2% of the profile) though due to the larger spot size than the size of the thin phosphate grains with needle-like texture (Fig. 3b) the concentrations resulted from a mixture with adjacent cholesterol grains. The layers composed of cholesterol were void of other elements than Ca, while both carbonate and phosphate in the core and in the thin outer layers of the sample were the carriers of a variety of elements, such as P, Na, Mg, Cu, Fe, Ni, and Mn (in decreasing order). Silver (average 1.44 and 0.27 ppm in carbonate and phosphate, respectively) and Pb (1.56 and 2.11 ppm, respectively) were scarce, whereas As, Cd, Co, and S were BDL in this sample (Fig. 3; Table 3). The phase distribution in the mixed cholesterol stone was similar to the one in pure cholesterol stone (Fig. 2A), hence pie diagram was not presented here. Calcium had good positive correlation with P (r = 0.628), Na (r = 0.845), and Mn (r = 0.858), while Cu (2600 and 2140 ppm, respectively) correlated with Fe (r = 0.938; 36.9 and 76.6 ppm, respectively), Mg (r = 0.738; 475 and 1850 ppm, respectively), Ag (r = 0.758; 1.44 and 0.29 ppm, respectively) and Pb (r = 0.841; 1.56 and 2.12 ppm, respectively).

3.3. Composite cholesterol stone

The composite cholesterol stone exhibited a visible layer structure with a core composed of pure cholesterol and a distinct layering with mixed and monomineralic outer bands (Fig. 4; [18]). The core presented notable resemblance to the pure cholesterol stones, and con-

Table 3
Bulk elemental concentrations of gallstones and the standards by solution ICP-MS/OES analysis. All values are given in ppm. (BDL = below detection limit; * non-certified values).

Sample/Standard	Ca	Mg	Na	P	S	Ag	As	Cd	Co	Cu	Fe	Ni	Mn	Pb
Pure cholesterol stone	27.6	11.8	1754	1075	177	BDL	BDL	BDL	BDL	2.32	8.08	BDL	0.33	0.01
Mixed cholesterol stone	30512	155	2178	2439	1250	0.15	BDL	0.009	BDL	26.0	22.3	BDL	15.2	0.34
Composite cholesterol stone	69260	880	2137	28155	825	BDL	BDL	0.013	BDL	15.2	6.57	BDL	10.0	1.45
Black pigment stone	10637	1427	16388	1636	9247	2.68	0.20	1.28	0.11	2860	1155	BDL	47.1	32.8
Carbonate Stone	221779	1321	2155	1573	854	BDL	0.006	BDL	0.05	26.0	94.5	2.07	554	1.2
Limit of detection	0.0001	0.0001	0.0002	0.002	0.003	0.1×10^{-4}	0.4×10^{-4}	0.4×10^{-4}	0.5×10^{-6}	0.5×10^{-4}	0.006	0.001	0.4×10^{-4}	0.5 ×
NIST1486 (certified)	265800	4660	5000*	123000	–	–	0.006*	–	–	0.8*	99	–	1.1	1.34
NIST1486 (measured)	273303	4116	6792	126541	–	–	0.008	–	–	0.8	105	–	1.2	1.27
Accuracy (%)	2.8	−11.7	35.8	2.9	–	–	33.3	–	–	0.0	5.6	–	9.1	−5.2
JLs-1 (certified)	393724	3655	14.4	129	123	0.0013*	0.15*	0.159	0.008	0.27*	125	0.36	13.9	0.22*
JLs-1 (measured)	432915	2855	23.5	153	153	BDL	0.15	0.157	0.006	0.27	129	0.41	14.6	0.12
Accuracy (%)	10.0	−21.9	63.6	18.9	24.5	–	0.0	−1.3	−25.0	0.0	3.6	13.9	5.0	−45.5

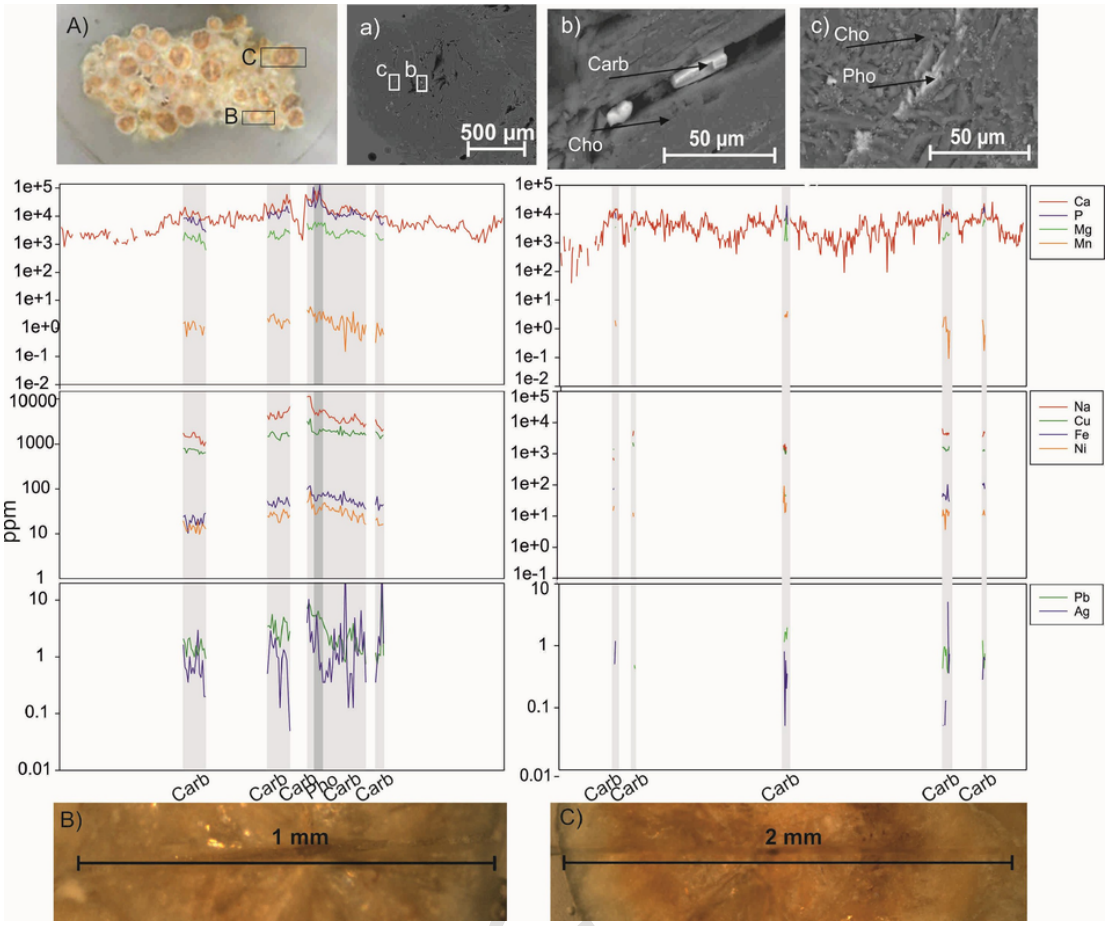

Fig. 1. A) Cross-section of the pure cholesterol stone and B–C) photographs of two grains showing the analyzed lines with their respective elemental LA-ICP-MS profiles covering the cross-sections, and a–c) back-scattered images of cholesterol (Cho), Ca carbonate (Carb), and Ca phosphate (Pho) grains in the respective sample. In the elemental profiles cholesterol is highlighted in white, Ca carbonate in light grey, and Ca phosphate in dark grey.

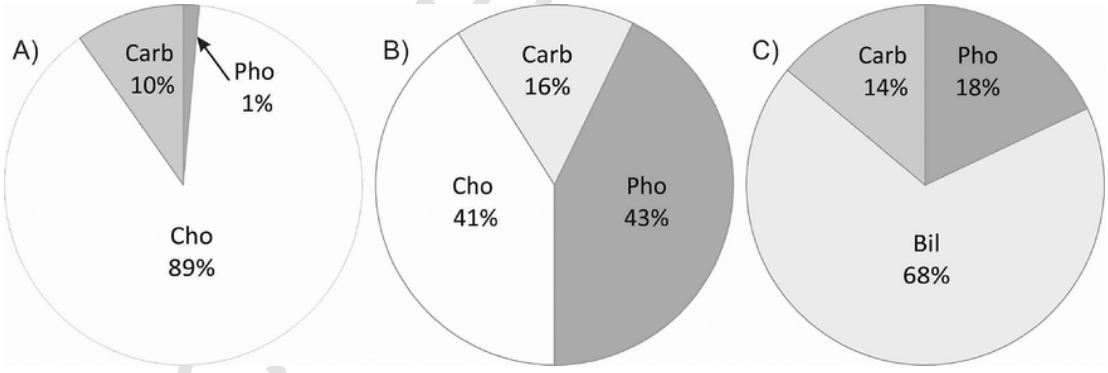

Fig. 2. Phase distribution in A) the pure cholesterol stone, B) the composite cholesterol stone, and C) the pigment stone. The pie diagrams represent the approximated portions of cholesterol (Cho), Ca carbonate (Carb), Ca phosphate (Pho), and Ca bilirubinate (Bil) in the analyzed LA raster lines.

tained merely scarce grains of Ca carbonate. The mixed layer containing varying amounts of cholesterol, bilirubinate, carbonate and phosphate (Fig. 4c) was covered by a homogeneous layer (approx. 1 mm in thickness; Fig. 4d) of hydroxyapatite [$Ca_5(PO_4)_3(OH)$] [18]. The ESEM-EDS analysis detected traces of Na and Mg in this layer (Fig. 4d). The outermost, whitish layer is also composed of phosphates (Fig. 4e). The distinct layering was also visible in the laser ablation profile where the characteristics of each layer were reflected as varying elemental abundances (Fig. 4). First, in the core Ca was the most abundant element with generally <0.5 wt.% and with a few peaks of Ca (up to 6 wt.%) corresponding to small grains of carbonates. Due to the small grain size of the carbonates, Ca concentrations were rather low for carbonates, which is a consequence of mixed analysis of cholesterol and carbonate grains. Other elements appeared merely in association with carbonate phases. The elemental abundances rose drastically in the layer with mixed composition first hitting a more homogeneous phosphate grain (average 66 wt.% of Ca and 11.5 wt.% of P) followed by a general decrease in Ca which probably corresponded to carbonate, cholesterol and Ca bilirubinate phases (Fig. 4). The concentrations of Ca and P together with Mg, Na, and Pb again increased in the hydroxyapatite layer and remained fairly stable until the end of the line in the whitish layer. In the latter, Cu, Fe, Mg, and Ni experienced a decrease with respect to

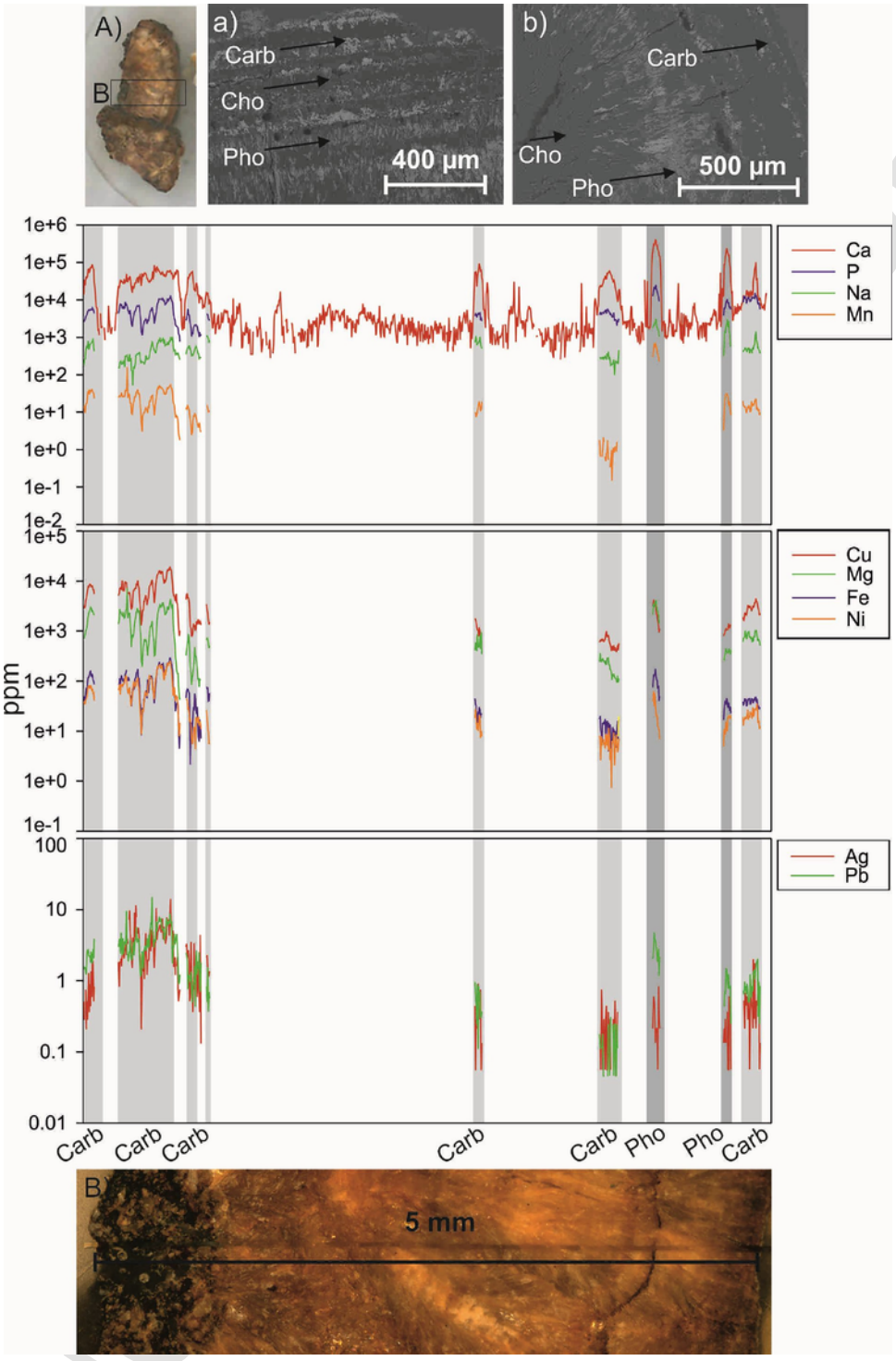

Fig. 3. A) Cross-section of the broken mixed cholesterol stone where the darker core of the gallstone is to the left and the surface of the calculus to the right on the analyzed line, B) the analyzed line with the respective elemental LA-ICP-MS profile covering the cross-section, and a–b) back-scattered images of cholesterol (Cho), Ca carbonate (Carb), and Ca phosphate (Pho) grains in the a) core and b) outer layers of the sample. In the profile cholesterol is highlighted in white, Ca carbonate in light grey, and Ca phosphate in dark grey.

hydroxyapatite layer. As a whole, in the composite cholesterol stone, Ca correlated positively with P (r = 0.635), Mg (r = 0.725), and Na (r = 0.731), while P exhibited good correlations with Fe (r = 0.685; average 30.7 and 85.9 ppm in carbonate and phosphate, respectively), Mn (r = 0.647), and Pb (r = 0.765; 4.81 and 17.2 ppm, respectively). Lead seemed to be enriched in phosphate phases, hence it was more abundant in the composite cholesterol stone than in the other two types of cholesterol stones. Copper (420 and 413 ppm, respectively) on the other hand presented positive correlations with Fe (r = 0.609) and Ni (r = 0.718; 3.29 and 3.24 ppm, respectively). Other elements, such as Ag, As, Cd, Co, and S are not shown in Fig. 4 as they were extremely scarce or BDL (Table 3).

Cholesterol occupied 41% of the ablated line, whereas phosphate and carbonate covered 43% and 16%, respectively (Fig. 2B). Based on the LA profiles, bilirubinate in the mixed layer could not be distinguished from carbonate phases due to the small grain size and the in-

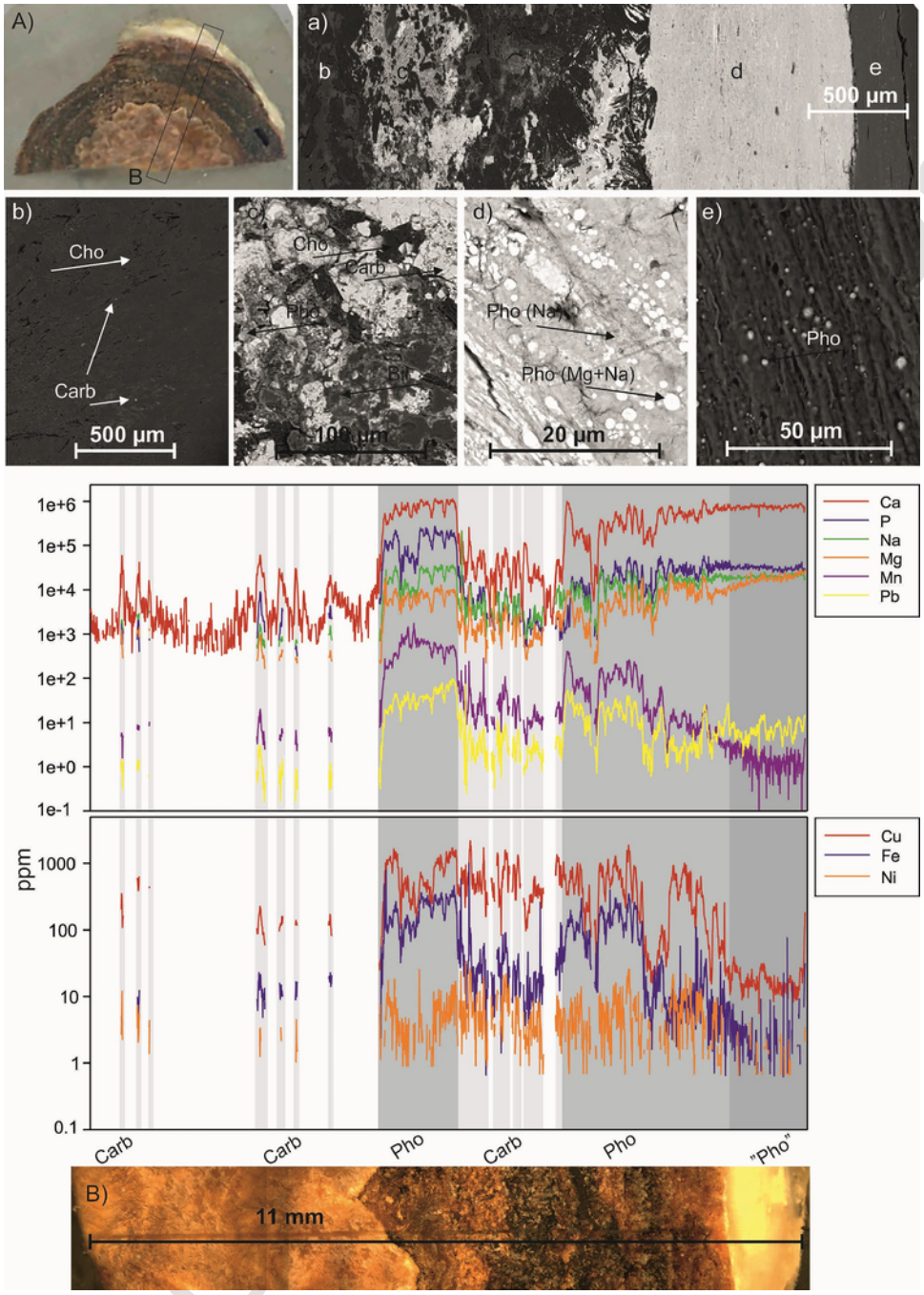

Fig. 4. A) Cross-section of the cut composite cholesterol stone, B) the analyzed line with the respective elemental LA-ICP-MS profile covering the cross-section, and a–e) back-scattered images of the varying layers of the sample with cholesterol (Cho), Ca bilirubinate (Bil), Ca carbonate (Carb), and Ca phosphate (Pho) grains, some of which contain Mg and Na. a) represents the cross-section of the sample, in which b) corresponds to cholesterol core, c) mixed layer of cholesterol, bilirubinate, Ca carbonate, and Ca phosphate, d) monomineralic hydroxyapatite, and e) outer crust with phosphate nodules. In the profile cholesterol is highlighted in white, Ca carbonate in light grey, and Ca phosphate in dark grey. The phosphate layer ("Pho") to the right (corresponding to Fig. 4e) has a band highlighted with slightly darker tone to distinguish the whitish phosphate crust.

ter-grown texture of the phases hence the possibly ablated bilirubinate grains are included in the estimation of carbonates.

3.4. Black pigment stone

The black pigment stones were principally composed of Ca bilirubinate and smaller amounts of Ca phosphate and Ca carbonate (Fig. 5; [18]). Roughly 32% of the ablated raster line corresponded to phosphate and carbonate phases which had >12 wt.% of Ca (Figs. 2C and 5). The highest P peaks (up to 18 wt.%) with high Ca peaks (up to 60 wt.%) were assumed to correspond to phosphate covering approximately 18% of the analyzed line and leaving 14% to the carbonate phases (Fig. 2C). The rest of the analyzed raster line, 68%, corresponded to Ca bilirubinate which exhibited abundant yet notably lower concentrations of Ca (approx. 10 wt.%) and considerably less P in comparison to the carbonate and phosphate phases (Figs. 2C and 5). Calcium, P, Mn, Na, Pb, and Cd, in order of abundance, were found in phosphate phases (Fig. 5). Phosphorous (r = 0.947), Mn (r = 0.964), Pb (r = 0.888; 132, 280, and 660 ppm, in bilirubinate, carbonate and phosphate, respectively), and Cd (r = 0.887; average 1.42, 5.45, and

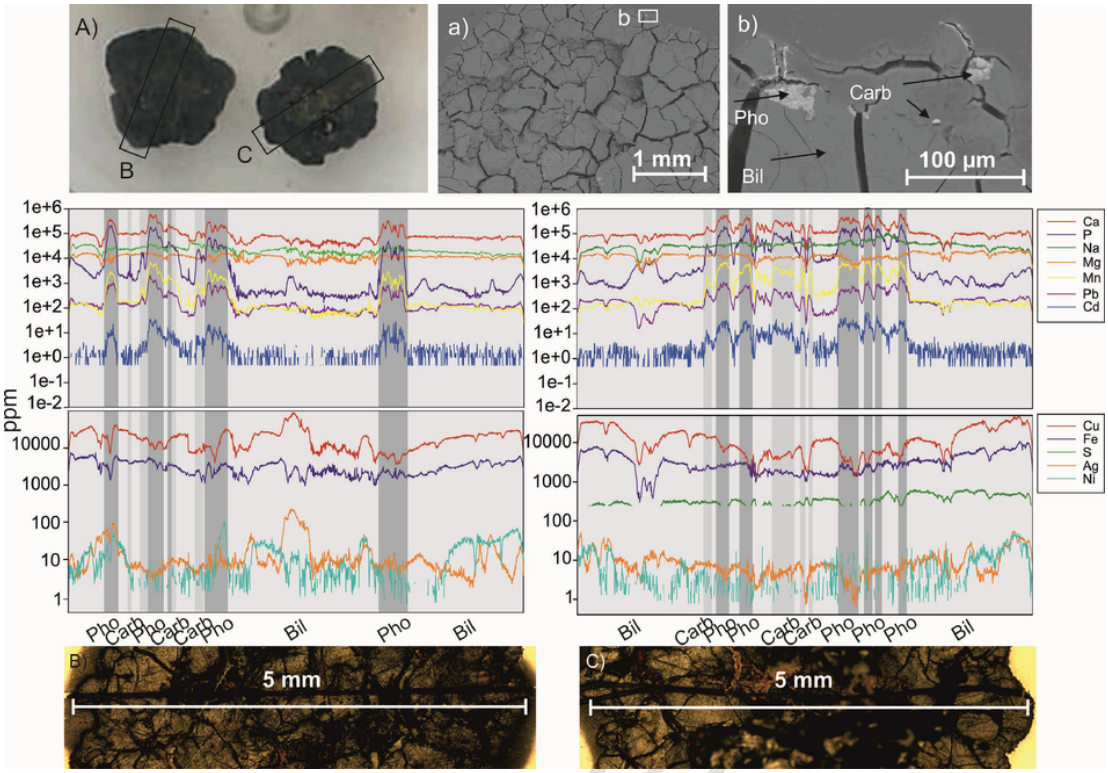

Fig. 5. A) Cross-sections of the black pigment stones, B–C) photographs of two grains showing the analyzed lines with their respective elemental LA-ICP-MS profiles covering the cross-sections, and a–b) back-scattered images of Ca bilirubinate (Bil), Ca carbonate (Carb), and Ca phosphate (Pho) grains in the respective samples. In the profiles Ca biliruninate is highlighted in light grey, Ca carbonate in medium grey, and Ca phosphate in dark grey.

17.4, respectively) exhibited very good positive correlations with Ca. Furthermore, Na exhibited elevated and fairly constant concentrations across the analyzed lines with a positive correlation with Ca (r = 0.532). Copper (2.0 wt.%, 1.3 wt.%, and 0.7 wt.%, respectively), on the contrary, presented negative correlation with Ca (r = −0.331) and P (r = −0.377), but other elements, such as Ni (r = 0.502; 10.1, 5.61, and 3.26 ppm, respectively) and Ag (r = 0.691; 16.2, 10.2, and 8.03 ppm, respectively) appeared in association with elevated Cu concentrations (>1.5 wt.%) preferentially in Ca bilirubinate. Cobalt presented extremely low concentrations (0.49, 0.52, and 0.50 ppm, respectively), whereas As was generally BDL, hence these elements are not shown in Fig. 5. Iron (3486, 2903, and 2594 ppm, respectively), Mg, and S did not exhibit clear affinity for any of the phases. For the most part, concentrations of S were BDL (300 ppm).

3.5. Carbonate stone

The carbonate stone was principally composed of Ca carbonate and cholesterol, but bilirubinate was detected as minor phase (Fig. 6; [18]). The elemental profile highlights the abundance of carbonate phases (Fig. 6). The higher peaks of Ca (generally >30 wt.% and up to 70 wt.%) were assumed to correspond to pure carbonate phases which occupy 61% of the analyzed raster line. On the other hand, merely few pronounced negative peaks of Ca in the absence of other elements can be observed where the laser hit larger cholesterol grains (Fig. 6). Cholesterol accounts for 8% of the profile. The peak downs in between carbonate grains were associated with the uneven surface where the laser probably hit small grains of cholesterol or bilirubinate or cracks (31% of the profile). This resulted in a mixture of phases, hence phase distribution pie diagram is not shown for carbonate stone. The overall Ca concentrations showed good, positive correlation with Mg (r = 0.638), Mn (r = 0.565), and Na (r = 0.753), while P (r = 0.160) was not dependent on Ca. Copper (r = −0.511; average 540 ppm in overall) and Ni (r = −0.459; 4.11 ppm), on the contrary, exhibited a significant negative correlation with Ca, but Cu correlated with Ni (r = 0.781) and Fe (r = 0.331; 127 ppm). In the pure carbonate phases, Ca had a slightly weaker though significant correlation with Mg (r = 0.435) and Na (r = 0.640). Besides As, Cd, Co, and S which were generally BDL, Ag (1.69 ppm) and Pb (4.11 ppm) exhibited very low concentrations, and were not clearly correlated with other elements.

4. Discussion

4.1. Metal affinities of different gallstone phases

The bulk metal abundances increased in the studied gallstones in the following order: pure cholesterol stone, mixed cholesterol stone, carbonate stone, composite cholesterol stone, and black pigment stone (Table 3). Previous studies have presented bulk concentrations of trace elements, e.g. using bulk analysis after acid digestion or X-ray Fluorescence. According to these results as well, pigment gallstones are the most enriched in metals such as Ca, Cu, Fe, Mg, Mn, and Zn [9–12,23]. However, these studies do not reveal which phases are the main hosts of metals in gallstones. Additionally, Parviainen et al. [18] documented the presence of metal nodules in gallstones, which are few microns in size and commonly contain different portions of e.g. Fe and Cu in association with other trace elements and for instance S. In the current study, LA-ICP-MS offered a more detailed insight to the metal distribution among the varying phases that compose the different gallstones. The low concentrations of metals in pure and mixed cholesterol stones were attributed to the abundance of cholesterol, which is void of metals except for Ca, and to the scarcity of metal bearing phases, such as carbonates and phosphates (Fig. 2A). The elemental distribution depicted in Fig. 1, highlights that carbonates and phosphates are the prin-

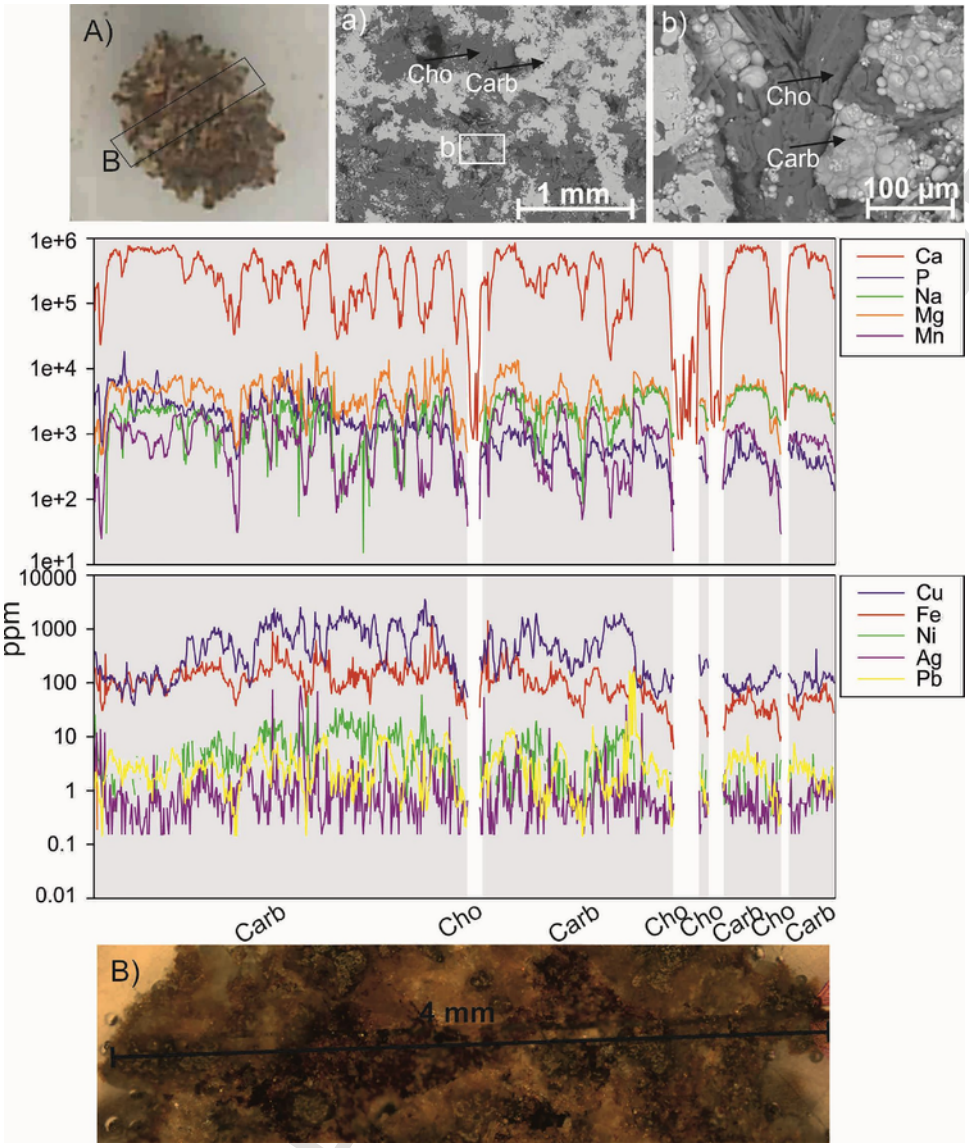

Fig. 6. A) Cross-section of the carbonate stone, B) the analyzed line with the respective elemental LA-ICP-MS profile covering the cross-section, and a–b) back-scattered images of cholesterol (Cho) and Ca carbonate (Carb) grains in the respective sample. In the profile Ca carbonate is highlighted in light grey and cholesterol in white.

cipal carriers of trace elements in pure cholesterol stones. The composite cholesterol stone presented a core similar to the pure cholesterol stone, but the outer layers, composed principally of Ca phosphates and carbonates, were rich in Ca and trace elements. Additionally, phosphate was the major carrier of P, Na, Mg, Mn, Fe, and Pb (in order of abundance; Fig. 4). On the contrary, Cu and Ni were distributed more evenly between carbonate and phosphate phases. The Ca carbonate phases of the carbonate stone were enriched in Mg, Na, and Mn, whereas P, Cu, Fe, and Ni behaved differently implying that carbonates are not their principal carriers. The elevated concentrations of metals in the black pigment stones were distributed throughout the sample surface appearing in the two major phases, namely in Ca bilirubinate and Ca phosphate. The phosphate was enriched in Ca, P, Na, Mn, Fe, Pb, and Cd (in order of abundance), whereas bilirubinate was enriched in Cu, Ni, and Ag (Fig. 5). Magnesium, Fe, and S were distributed more evenly over all of the phases with no clear preferences.

In other biomineralizations, phosphates may incorporate a variety of metals in their structure. For instance, the phosphate phases of urinary stones are enriched in Na, Mg, Sr, and Zn [17]. Moreover, elevated concentrations of Pb, Zn, Hg, Sb, Al, Sr, and Sn in human teeth dentine, composed of hydroxyapatite, have been detected in Chinese, Malay, and Indian people, which are attributed to exposure to environmental pollution [24]. Evident from the outer layers of the composite cholesterol stone and from the black pigment stones, phosphates have the highest affinity to immobilize Pb and Cd among the studied phases.

These results suggest that metals are retained from the bile in gallstones which preferentially are composed of carbonates, phosphates, or organic bilirubinate salts. In case of the pure cholesterol stones, cholesterol has no capacity to accumulate metals, and the metals are eliminated from human body through bile discharge instead of being accumulated in these biomineralizations. On the contrary, the pigment stones are most enriched in a variety of metals. This work elucidates the trace element behavior in the gallstone formation and gives new perspectives to use these biomineralizations as proxies for exposure to metal pollution.

4.2. Significance of the LA-ICP-MS results

Although few articles have attempted to constrain the elemental distribution in gallstones using scanning electron microscope

[18,25–27], to our knowledge, this is the first time LA-ICP-MS is applied to natural gallstones in such detail, and the elemental concentrations are related to mineral phase composition of these biomineralizations. On the other hand, the elemental abundances of kidney stones by LA-ICP-MS have been previously studied on powdered and homogenized samples through pressed pellets and on cross-section of calculi [15–17]. The combination of mineral identification, bulk solution ICP-MS/OES, and LA-ICP-MS analyses in this work allowed a detailed interpretation of metal abundances and metal partitioning in different phases constituting varying types of gallstones.

The semi-quantitative elemental abundances constrained by LA-ICP-MS were generally in good agreement with the bulk solution ICP-MS/OES results (Table 3). For example, Ca exhibited the lowest concentrations in the pure cholesterol stone and was richer in the rest of the sample types according to the increasing abundance of bilirubinate, carbonate, and phosphate phases in agreement with the LA profiles (Figs. 1, 3–6). Silver, As, Cd, Co, Ni, and Pb were generally very scarce or BDL in the bulk analyses, and exhibited consistent, extremely low concentrations or were BDL under LA, with the exception of pigment stones. However, as the analyzed LA profiles represent merely a small portion of each sample, some inconsistencies between the LA and bulk results may be observed. For instance, some scarce elements (such as Ag and Ni) were BDL in the homogenized bulk sample but were present at low concentrations in specific phases (carbonate, phosphate, or bilirubinate) in the LA profile of the sample cross-sections. On the contrary, for example S was BDL (300 ppm) under LA-ICP-MS in nearly all of the gallstone cross-sections except for pigment stones, but was concentrated in hundreds to thousands of ppm in the corresponding bulk analysis (Table 3). This may be due to nugget effect as possible presence of S-bearing metal nodules or other minor phases in the bulk samples [18] which are not represented in the LA profile on the sample cross-section.

5. Conclusions

Chronic exposure to metal pollution, for instance derived from metal mining, may have an adverse effect on human health, and metals are known to accumulate in the human body. This study presents the trace element affinities of five different types of gallstones, namely pure, mixed and composite cholesterol stones, pigment stone and carbonate stone. The LA-ICP-MS measurements on the gallstone cross-sections in combination with bulk solution ICP-MS/OES analyses revealed that cholesterol cannot retain any elements except for Ca. Ca phosphates on the other hand had the highest capacity to trap a variety of elements such as Na, Mg, Cu, Mn, Fe, Pb, and Cd. Also Ca carbonate phases exhibited high affinity to trap Mg, Mn, and Na, while Ca-bilirubinate was enriched in Cu, Ni, and Ag. These tendencies explain the varying bulk trace element concentrations in the different types of gallstones, where pure cholesterol stone was the most depleted while pigment stone, composed principally of bilirubinate and phosphate, was the most enriched in trace metals. The findings of this work give new insight to the trace element behavior in the gallstone formation and their possible use as environmental proxies for metal pollution in areas seriously affected by, for instance, mining or other industrial activities.

Conflicts of interest

The authors declare that there are no conflicts of interest.

Acknowledgements

The authors would like to show their gratitude to I. Martínez Segura for her assistance in sample preparation and laboratory work and to Dr. C.J. Garrido for his advice on the manuscript. Additionally, the authors thank the collaboration of the Department of Surgery and the Department of Pathology of the General Hospital of Riotinto. Dr. A. Parviainen and Dr. C. Marchesi acknowledge the 'Juan de la Cierva – Formación' (FJCI-2014-19582) and the 'Ramon y Cajal' (RYC-2012-11314) Fellowships, respectively, funded by the Spanish Ministry of Economy and Competitiveness (MINECO). Dr. C. Marchesi acknowledges funding from the "Junta de Andalucía" research group RNM-131, and Dr. R. Pérez-López recognizes funding from SCYRE project (CGL2016-78783-C2-1-R). The European Social Fund (ESF) and the European Regional Development Fund (ERFD) of the European Commission have co-funded fellowships and infrastructure grants used in this research.

References

[1] K. Szentmihályi, P. Sípos, A. Blázovics, P. Vinkler, M. Szilágyi, Concentration of biliary metal elements and gallstone formation in humans (cholelithiasis), Trace Elem. Electrolytes 19 (3) (2002) 160–164.
[2] M. Kohlmeier, Chapter 11: minerals and trace elements, in: M. Kohlmeier (Ed.), Nutrient Metabolism 2nd Edition—Structures, Functions, and Genes, Academic Press, 2015, pp. 673–805, ISBN: 978-0-12-387784-0.
[3] Y. Sun, Z. Yang, G. Shen, Y. Zhou, X. Zhou, J. Wu, G. Xu, Progress in the study on the composition and formation mechanism of gallstone, Sci. China Ser. B: Chem. 44 (5) (2001) 449–456.
[4] S. Basu, M.K. Singh, T.B. Singh, S.K. Bhartiya, S.P. Singh, V.K. Shukla, Heavy and trace metals in carcinoma of the gallbladder, World J. Surg. 37 (2013) 2641–2646.
[5] S. Unisa, P. Jagannath, V. Dhir, C. Khandelwal, L. Sarangi, T.K. Roy, Population based study to estimate prevalence and determine risk factors of gallbladder diseases in the rural Gangetic basin of North India, HPB (Oxford) 13 (2011) 117–125.
[6] N. Suzuki, Y. Nakamura, N. Kobayashi, T. Sato, On metal elements in pure pigment gallstones, Tohoku J. Exp. Med. 16 (3) (1975) 233–240.
[7] X.-S. Zhou, G.-R. Shen, J.-G. Wu, W.-H. Li, Y.-Z. Xu, S.-F. Weng, R.D. Soloway, X.-B. Fu, W. Tian, Z. Xu, T. Shen, G.-X. Xu, E. Wentrup-Byrne, A spectroscopic study of pigment gallstones in China, Biospectroscopy 3 (5) (1997) 371–380.
[8] M. Suhara, K. Matsuda, K. Sera, Elemental concentrations of four types of human gallstones by PIXE analysis, Int. J. PIXE 08 (1998) 73, https://doi.org/10.1142/S0129083598000091.
[9] M. Ashok, T.R. Rautray, P.K. Nayak, V. Vijayan, V. Jayanthi, S. Narayana Kalkura, Energy dispersive X-ray fluorescence analysis of gallstones, J. Radioanal. Nucl. Chem. 257 (2) (2003) 333–335.
[10] A. Palchik, T.N. Moroz, Polymorph modifications of calcium carbonate in gallstones, J. Cryst. Growth 283 (2005) 450–456.
[11] T.R. Rautray, V. Vijayan, S. Panigrahi, Analysis of Indian pigment gallstones, Nucl. Inst. Methods Phys. Res. B 255 (2007) 409–415.
[12] L.S. Omer, Quantitative analysis in (33) traces metals in human gallstones by IC-PAES, Int. J. Chem. 3 (2) (2011) 105–110.
[13] R. Sharma, S. Soy, C. Kumar, S.G. Sachan, S.R. Sharma, Analysis of gallstone composition and structure in Jharkhand region, Indian J. Gastroenterol. 34 (1) (2015) 29–37.
[14] H. Weerakoon, A. Navaratne, S. Ranasinghe, R. Sivakanesan, K.B. Galketiya, S. Rosairo, Chemical characterization of gallstones: an approach to explore the aetiopathogenesi of gallstone disease in Sri Lanka, PLoS One 10 (4) (2015) https://doi.org/10.1371/journal.pone.0121537, e0121537.
[15] K. Proksova, K. Novotny, J. Kaiser, M. Galiova, T. Vaculovic, V. Kanicky, Study of elemental distribution in urinary stones by laser ablation inductively coupled plasma mass spectrometry (LA-ICP-MS), J Biochem. Tech. 2 (5) (2010) S106–S107.
[16] K. Štěpánková, K. Novotný, M. Vašinová Galiová, V. Kanický, J. Kaiser, D.W. Hahn, Laser ablation methods for analysis of urinary calculi: comparison study based on calibration pellets, Spectrochim. Acta Part B 81 (2013) 43–49.
[17] M. Vašinová Galiová, R. Čopjaková, R. Škoda, K. Štěpánková, M. Vaňková, J. Kuta, L. Prokeš, J. Kynický, V. Kanický, 2D elemental mapping of sections of human kidney stones using laser ablation inductively-coupled plasma-mass spectrometry: possibilities and limitations, Spectrochim. Acta Part B 100 (2014) 105–115.
[18] A. Parviainen, J.M. Suárez-Grau, R. Pérez-López, J.M. Nieto, C.J. Garrido, G. Cobo-Cárdenas, Combined microstructural and mineralogical phase characterization of gallstones in a patient-based study in SW Spain—implications for environmental contamination in their formation, Sci. Total Environ. 573 (2016) 433–443.
[19] C. Paton, J. Hellstrom, B. Paul, J. Woodhead, J. Hergt, Iolite Freeware for the visualisation and processing of mass spectrometric data, J. Anal. At. Spectrom. 26 (2011) 2508–2518, https://doi.org/10.1039/c1ja10172b.
[20] Iolite, Iolite 3 User's Manual, School of Earth Sciences the University of Melbourne, 2016.
[21] H.P. Longerich, S.E. Jackson, D. Günther, Inter-laboratory note. Laser ablation inductively coupled plasma mass spectrometric transient signal data acquisition and analyte concentration calculation, J. Anal. At. Spectrom. 11 (1996) 899–904.
[22] D. Howell, W.L. Griffin, N.J. Pearson, W. Powell, P. Wieland, S.Y. O'Reilly, Trace element partitioning in mixed-habit diamonds, Chem. Geol. 355 (2013) 134–143.

[23] N.A. Channa, F.D. Khand, M.Y. Khuhawar, M.I. Bhanger, Study of some metal element in four chemically different types of human gallstones, J. Chem. Soc. Pak. 26 (2) (2004) 123–126.
[24] K. Asaduzzaman, M.U. Khandaker, N.U.B. Baharudin, Y.B.M. Amin, M.S. Farook, D.A. Bradley, O. Mahmoud, Heavy metals in human teeth dentine: a bio-indicator of metals exposure and environmental pollution, Chemosphere 176 (2017) 221–230.
[25] J.M. Bravo Arredondo, A bulk and located analysis of gallstones, Int. J. Sci. Eng. Res. 4 (6) (2013), ISSN 2229–5518.
[26] A. Iordanidis, J. Garcia-Guinea, C. Giousef, A. Angelopoulos, M. Doulgerakis, L. Papadopoulou, Characterization of gallbladder stones from cholelithiasis patients of Northern Greece, using complementary techniques, Spectrosc. Lett. 46 (2013) 301–306.
[27] S. Cavalu, A. Popa, I. Bratu, G. Borodi, A. Maghiar, New evidences of key factors involved in silent stones etiopathogenesis and trace elements: microscopic, spectroscopic,and biochemical approach, Biol. Trace Elem. Res. 168 (2) (2015) 311–320.